THE JOURNAL OF PHYSICAL CHEMISTRY B

Article

pubs.acs.org/JPCB

Amino Acid Anions in Organic Ionic Compounds. An ab Initio Study of Selected Ion Pairs

A. Benedetto,[†] E. Bodo,*[,‡] L. Gontrani,*[,‡,§] P. Ballone,[∥,⊥] and R. Caminiti[‡]

[†]School of Physics, University College Dublin, Dublin 4, Ireland

[‡]Department of Chemistry, Università di Roma "La Sapienza", 00185 Roma, Italy

[§]CNR-ISM, Via del Fosso del Cavaliere 100, 00133 Roma, Italy

[∥]Center for Life Nano Science @Sapienza, Istituto Italiano di Tecnologia (IIT), 00161 Roma, Italy

[⊥]Department of Physics, Università di Roma "La Sapienza", 00185 Roma, Italy

Supporting Information

ABSTRACT: The combination of amino acids in their deprotonated and thus anionic form with a choline cation gives origin to a new and potentially important class of organic ionic compounds. A series of such neutral ion pairs has been investigated by first principle methods. The results reveal intriguing structural motives as well as regular patterns in the charge distribution and predict a number of vibrational and optical properties that could guide the experimental investigation of these compounds. The replacement of choline with its phosphocholine analogue causes the spontaneous reciprocal neutralization of cations and anions, taking place through the transfer of a proton between the two ions. Systems of this kind, therefore, provide a wide and easily accessible playground to probe the ionic/polar transition in organic systems, while the easy transfer of H^+ among neutral and ionic species points to their potential application as proton conductors. The analysis of the ab initio data highlights similarities as well as discrepancies from the rigid-ions force-field picture and suggests directions for the improvement of empirical models.

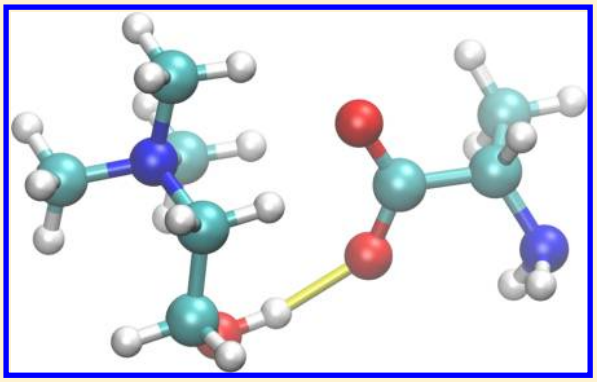

I. INTRODUCTION

The remarkable properties of room-temperature ionic liquids (RTIL),[1,2] including their low volatility, thermal stability, and versatility, have raised high expectations for industrial applications, fueling a vast research effort.[3]

The low environmental impact of these compounds, arguably the first and foremost reason of their widespread appeal,[4] could perhaps be further reduced by designing ionic liquids made entirely of bioorganic species, whose affinity for biological molecules, moreover, could open new vistas in pharmacology applications.[5,6]

These ideas have found a first and partial realization in the recent synthesis and characterization of ionic liquids made by amino acid anions in combination with cations such as 1-ethyl-3-methylimidazolium,[7−9] tetra-butylphosphonium,[10] and so on, already extensively used in more traditional RTILs.

We focus here on a different family of ionic compounds, consisting of amino acid anions joined to a protonated choline cation ($[Chol]^+$), which has already been used in combination with inorganic anions,[11−13] and represents an essential component of deep-eutectic mixtures, whose ionic conductivity, viscosity, and surface energies are similar to those of imidazolium-based RTIL.[14]

At variance from previous cation choices, choline plays an important role in metabolism and is present in a wide variety of living organisms, and thus ionic liquids made of $[Chol]^+$ and deprotonated amino acids provide a more comprehensive implementation of the research plan briefly outlined above. Moreover, like many other organic molecules, choline can be modified into a variety of analogue species, adding one more dimension to the choice of amino acid-based ionic systems. Last, but not least, amino acid-based ionic liquids could provide a privileged model to investigate the mutual relation of proteins and RTILs,[15−17] enhancing our understanding of a subject of interest for biotechnology and for catalysis.

Compounds of this type have been synthesized, and their macroscopic and microscopic properties are being measured and characterized.[18] To ease and complement the experimental effort, we present here the results of density functional computations for a short series of ion pairs, consisting of a choline cation ($[Chol]^+$) and eight different amino acid anions, represented by alanine $[Ala]^-$, valine $[Val]^-$, serine $[Ser]^-$, cysteine $[Cys]^-$, aspartic acid $[Asp]^-$, asparagine $[Asn]^-$,

Received: December 16, 2013
Revised: February 3, 2014
Published: February 5, 2014

phenylalanine $[Phe]^-$, and histidine $[His]^-$, in their deprotonated form. These species have been selected in such a way to cover all the major families of the most common (proteinogenic) amino acids.

For each neutral ion pair, we determine the geometry, the charge distribution, vibrational properties, and low-lying singlet and triplet excitation energies of the gas-phase species. Moreover, to explore the effect of temperature and of a condensed environment, we carry out ab initio molecular dynamics simulations on small neutral clusters with up to four ion pairs. The results highlight an intriguing picture of geometrical motifs conserved along the amino acid sequence, and a variety of different arrangements that could be rationalized in terms of the polarity and hydrogen bonding capability of the amino acid residue.

To assess the role of the cation, additional computations have been performed for a phosphocholine cation ($[PhChol]^+$) joined to the $[Ala]^-$, $[Ser]^-$, and $[Asp]^-$ anions. Somewhat surprisingly, the replacement of choline with its close phosphocholine relative causes the spontaneous neutralization of the system, taking place through the transfer of the proton shared in the hydrogen bond connecting the cation and the anion. Such a chemical transformation, which corresponds to an ionic to polar transition, leaves almost unchanged the geometry and most properties of the resulting molecular pair, bound by a strong hydrogen bond, and by even stronger dipole−dipole interactions. The computational and experimental determination of cohesive, structural, and especially transport properties across the $[Chol]^+$ and $[PhChol]^+$ family of compounds, therefore, could open a new chapter in the decades-long investigation of protic ionic liquids.[19]

Besides providing support to the experimental activity, the ab initio data could be used to check, refine, and extend generic force-field models[20−22] for these and similar compounds, intended for large-scale simulations of bioorganic RTIL's based on amino acids and of mixed RTIL/biological systems.

The richness and variety of bioorganic molecules suggest that the results of this study and of previous experimental investigations[7−10] represent only the first steps into a vast and still unexplored territory, in which the interplay of ionic/polar bonding, amphoteric character, and affinity for biological structures and processes could greatly extend the already vast range of RTIL applications.

II. MODEL AND METHOD

Density functional theory (DFT) with generalized gradient and hybrid approximations[23] for the exchange-correlation energy represents the primary theoretical framework for our study. Computations on selected systems and properties have been carried out using MP2 to check the accuracy and reliability of the DFT results.

Independent electron (Kohn−Sham) orbitals have been represented using plane waves or Cartesian−Gaussian functions.

Plane wave computations have been carried out using the CPMD package,[24] with soft norm-conserving, nonlocal pseudopotentials,[25] and a kinetic energy cutoff of 80 Ry for the orbitals and 320 Ry for the density. All neutral species, including ion pairs and small clusters, have been enclosed in a cubic box of 24 Å side, periodically repeated in space. A cubic box of 26 Å side has been used for ionic species, and, in this case, open, i.e., nonperiodic, boundary conditions[26] have been applied. The exchange and correlation energy has been computed using the Perdew−Burke−Ernzerhof (PBE) approximation,[27] with the semiempirical correction of ref 28, to account for dispersion interactions, defining what in the following will be referred to as PBE+vdW (vdW = van der Waals).

The 6-311+G(d) Gaussian basis set has been employed to carry out all electron computations with the Gaussian09 package.[29] In this case, the exchange and correlation energy and potential have been approximated by the M06-2X functional,[30] supplemented by the D3 version of the empirical dispersion corrections (M06-2X/D3).[31,32] D3, in turn, represents a refinement of the model used in the plane wave (CPMD) computations, whose parameters have been tuned to optimize the matching with hybrid functionals. The same localized basis and Gaussian09 package have been used for the MP2 test computations.

The methods and packages listed in the previous paragraphs have been applied to search for the ground-state structure by simulated annealing (CPMD) and by a variant (GEDIIS)[33] of the direct inversion in the iterative subspace algorithm (Gaussian09), to compute cohesive energies, atomic charges (CPMD), and molecular dipole moments. Atomic charges, in particular, have been estimated using the electrostatic potential fitting (ESP)[34] as implemented in CPMD, and by the natural bond orbital[35−37] (NBO) analysis (Gaussian09). The comparison of the ESP and NBO charges is of particular interest, since the two methods display complementary strengths and limitations. With respect to NBO, the ESP approach does not depend on the choice of atomic orbitals, and requires the ground-state electron density as its only input. However, the ESP fit of the electrostatic potential becomes ill-defined in the case of compact molecules, with atoms buried in its interior. The NBO analysis does not suffer from this limitation, but it relies on a rather idealized model of bonding that might not cover the full range of possibilities found in real systems. In favorable cases, the atomic charges obtained by the two methods agree fairly well, and in these cases their common value can be considered a reliable characterization of the molecular charge distribution.

The NBO approach has been used again to quantify the strength of hydrogen bonds in the systems that we investigated. It might be useful to emphasize that the NBO value of the bond strength does not correspond to the potential energy variation upon forming or breaking a hydrogen bond but represents a perturbative estimate of the delocalization contribution to the binding energy. Once again, it relies on a simplified bonding−antibonding picture of the electronic structure, and it is used here as a relative scale of hydrogen bond intensity, whose correlation with hydrogen bond energies has been documented in the literature.[35−37]

The energy and displacement pattern of vibrational normal modes according to PBE+vdW have been determined by diagonalizing the dynamical matrix of the system computed by CPMD. The second derivatives of the energy with respect to the atomic positions, entering the definition of the dynamical matrix, have been approximated by finite differences. Standard vibrational analysis implemented in Gaussian09 has been used to characterize the harmonic dynamics of all of the species, as given by the M06-2X/D3 hybrid functional.

CPMD, again with the PBE+vdW approximation, has been applied to carry out molecular dynamics simulations in the microcanonical ensemble for a few neutral clusters and to probe activation energy barriers opposing intra- and intermolecular

proton transfers using geometric constraints on selected atom pairs, as implemented in CPMD.[38]

All of the ground-state species are spin-unpolarised closed shell systems. Spin polarization, however, enters the determination of excited-state properties by the Delta self-consistent-field (ΔSCF) approach.[39] We compute, in particular, the energy difference separating the singlet ground state from the lowest energy singlet and triplet states. All of the excited-state computations presented in subsequent text have been carried out within the PBE+vdW/plane wave approach (CPMD) and concern *vertical* excitations, taking place at the ground-state geometry.

The triplet-state energy, E_T, can be estimated directly, using the spin-polarized version of the PBE+vdW exchange-correlation functional. The computation of the energy of the lowest lying singlet is slightly more involved, because this state cannot be expressed as a single product of a spin up and a spin down determinant. To overcome this problem, we used the two-step approach of von Barth;[40] i.e., we first compute the energy E_m of the state obtained upon promoting one electron to the lowest energy empty orbital of the same spin. This is a mixed state; i.e., it is an eigenstate of S_z ($\langle S_z \rangle = 0$), but a combination of different S^2 states. However, the energy of the first singlet excited state can be estimated by the combination of E_T and E_m:

$$E_S = 2E_m - E_T \quad (1)$$

Hence, the singlet excitation energy is

$$\Delta E_S = E_S - E_{GS} = (E_m - E_{GS}) + (E_m - E_T) \quad (2)$$

where E_{GS} is the energy of the singlet ground state (see also ref 41).

As a way to predict excitation energies, the ΔSCF approach is certainly better justified than the analysis of Kohn−Sham eigenvalues, at least for the lowest energy excitations of singlet and triplet spin multiplicity. However, it remains an approximate method whose accuracy is uncertain, even though in the case of relatively simple organic compounds it has generally been found to be within 0.25 eV from experimental results.[42] Computations of optical properties by TD-DFT[43] and by Bethe Salpeter on GW orbital energies[44] are under way, and the results will be published elsewhere.

III. RESULTS

As anticipated in the Introduction, computations have been carried out for eight ionic compounds made of a choline cation, joined to the deprotonated and thus anionic form of alanine, serine, cysteine, valine, phenylalanine, aspartic acid, asparagine, and histidine. Additional computations have been performed for three analogue compounds ([PhChol][Ala], [PhChol]-[Ser], and [PhChol][Asp]) in which the $[Chol]^+$ cation is replaced by $[PhChol]^+$. The schematic structure of the cations and a few of the anions is shown in Figure 1.

For reasons of convenience, the bulk of our computations has been carried out within the generalized gradient correction approach, with hybrid functionals, and to a lesser extent MP2, used as a benchmark. This choice is reflected in the organization of the present section, in which, unless stated otherwise, results refer to the PBE+vdW computations. In most cases, we consider a single ion pair in the gas phase, although a few computations for small neutral clusters have been carried out as well.

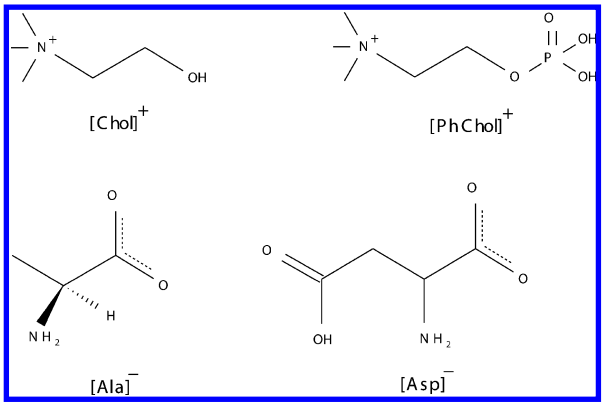

Figure 1. Schematic structure of the $[Chol]^+$, $[PhChol]^+$ cations and a few representative anions ($[Ala]^-$ and $[Asp]^-$).

The $[Chol]^+$ cation is a relatively simple molecule of ∼6 Å diameter, with limited internal flexibility represented primarily by the orientational freedom of the OH group. The analysis of the charge distribution via the ESP decomposition[34] shows a sizable positive charge (∼1.1*e*) located on the nitrogen atom, a fairly large negative charge (∼−0.65*e*) on the oxygen atom, to some extent compensated by the positive charge (+0.44*e*) of the hydrogen atom covalently bonded to it. The balance of charge needed to provide choline with the +1*e* net charge is distributed among its CH_3 and CH_2 groups.

The two major centers of interaction, represented by the oxygen and nitrogen atoms in choline, are separated by 3.01 Å, and this length is important in deciding the orientation and strength of the choline binding to amino acids. At variance from simple cations such as Na^+ or K^+, therefore, choline is a fairly large species, with a net charge, but also with a marked polarity due to the uneven distribution of positive and negative charge on its different groups. Moreover, $[Chol]^+$ is able to form a short-ranged and directional hydrogen bond whenever its OH apical group approaches another electronegative atom.

From the point of view of vibrational spectroscopy, the gas-phase choline cation is characterized by an easily identifiable O−H stretching mode at 3698 cm^{-1} having a large dipolar signature, well-separated from 13 C−H stretching modes at frequencies ranging from 2920 to 3110 cm^{-1}. This simple picture changes significantly whenever the OH group is engaged in a hydrogen bond, decreasing the frequency of its stretching mode by up to 900 cm^{-1}, depending on the strength of the hydrogen bond.

The phosphocholine cation is obviously a larger, more complex and more flexible species than choline. The incorporation of phosphate into the choline cation does not change drastically the distribution of charge among the atoms and distinct functional groups. The ESP charge on the nitrogen atom, in particular, is again ∼1.1*e*, and the charge on each of the two OH groups is nearly the same as that for the single hydroxyl of choline. The uneven distribution of charge on H_2PO_4, however, introduces additional polarity into this species and affects its geometry, since the two unprotonated oxygens feel the attraction of the positively charged N atom and position themselves at the shortest distance (∼3.8−4.0 Å) from this atom compatible with the steric hindrance of the CH_2 and CH_3 groups directly bonded to nitrogen. As a result, the interaction sites available to bind amino acids are only a bit farther than in choline, since the nitrogen atom is only 4.36 Å

dx.doi.org/10.1021/jp412281n | J. Phys. Chem. B 2014, 118, 2471−2486

Table 1. Binding Energy, E_b, of Neutral Ion Pairs[a]

	[Ala]$^-$	[Val]$^-$	[Ser]$^-$	[Cys]$^-$	[Asp]$^-$	[Asn]$^-$	[Phe]$^-$	[His]$^-$
[Chol]$^+$	106.0	104.6	104.9	104.6	102.7	104.9	102.7	93.3
	(107.7)	(106.3)	(106.9)	(106.3)	(104.9)	(106.8)	(104.3)	(94.8)
[PhChol]$^+$	113.8		110.2		103.2			
	(115.4)		(112.2)		(104.8)			

[a]The zero point energy contribution is included. The value excluding this term is given in in parentheses. Energies in kilocalories per mole per ion pair.

Table 2. Selected Structural Parameters of the Neutral Ion Pairs[a]

	[Ala]$^-$	[Val]$^-$	[Ser]$^-$	[Cys]$^-$	[Asp]$^-$	[Asn]$^-$	[Phe]$^-$	[His]$^-$
				[Chol]$^+$				
$O_{A1}-H_{Ch}$	1.59	1.59	1.63	1.65	1.71	1.65	1.60	1.63
$O_{A1}-O_{Ch}$	2.62	2.62	2.65	2.66	2.70	2.66	2.62	2.65
$O_{A1}-H-O_{Ch}$	179	179	173	170	168	175	177	173
$O_{Ai}-N_{Ch}$	3.28	3.30	3.36	3.44	3.45	3.34	3.29	3.35
				[PhChol]$^+$				
$O_{A1}-H_{PhCh}$	1.05		1.06		1.07			
$O_{A1}-O_{PhCh}$	2.55		2.52		2.51			
$O_{A1}-H-O_{PhCh}$	171		172		173			
$O_{Ai}-N_{PhCh}$	3.66		3.68		3.68			

[a]The naming of atoms follows Figure 2. Distances are in angstroms and angles in degrees.

from the closest hydroxyl oxygen and 5.59 Å from the other one.

Vibrational properties of choline and phosphocholine are similar, with fairly predictable differences due to characteristic modes of the bulky phosphate unit. H_2PO_4 rotations at ∼200 cm^{-1}, and O−P−O bending at ∼300−500 cm^{-1}, in particular, enhance the phosphocholine density of states at relatively low frequency. P−O stretching modes, at ∼700−1000 cm^{-1}, mark another difference in the vibrational spectra of choline and phosphocholine that, however, are still recognizable as closely related.

To complete this short overview of the cation properties, we mention that, according to our ΔSCF computations carried out within PBE+vdW, choline has a large optical gap of 8.06 eV (singlet vertical excitation), that is somewhat reduced to 6.80 eV in phosphocholine.

These first results on choline and phosphocholine provide the setting for the characterization of their interaction with the amino acid anions.

A. Binding Energies and Structural Trends. Low-energy structures have been determined primarily by simulated annealing using the CPMD package[24] to carry out molecular dynamics on the Born−Oppenheimer surface. The local stability of the proposed ground-state structures has been confirmed by the computation of harmonic vibrational frequencies, and the global relevance of the minima found by CPMD has been tested by additional geometry optimization runs carried out by Gaussian09.

The first relevant observation revealed by our computations is the remarkable strength of the cation−anion binding energy, E_b, and its relative insensitivity with respect to the amino acid choice (see Table 1, showing the binding energy per ion pair with respect to the separated and relaxed ions). Since the Coulomb attraction is obviously decreased by the large size of the ions, the binding energy comparable to or even larger than that of much smaller ions such Na^+ and Cl^- points to a sizable contribution from hydrogen bonding, polar, and dispersion interactions. The nearly constant value of E_b, moreover, suggests a remarkable conservation of distances and relative orientations of interacting groups along the sequence of these homologous compounds.

The ab initio results for the ground-state structure confirm that the cation−anion docking geometry is nearly the same for all of the [Chol]$^+$ compounds that we considered, as shown by the data reported in Table 2. Each ion pair, in particular, displays a hydrogen bond connecting the choline oxygen (donor) to one of the carboxylate oxygens (O_{A1}, acceptor). The partner carboxylate oxygen (O_{A2}) points toward the choline nitrogen, apparently because of the Coulomb attraction arising from its positive charge. The strength of the hydrogen bond is highlighted by the short separation of the $O_{Ch}-O_{A1}$ distance, by its low variation along the sequence (from d_{OO} = 2.62 Å in [Chol][Ala] and [Chol][Val] to d_{OO} = 2.70 Å in [Chol][Asp]), by its remarkable linearity (see Table 2), and by the drastic effect it has on the stretching frequency of the choline $(OH)_{Ch}$ termination, as discussed in section IIB.

In the ion pairs, the primary NH_2 amino group does not interact directly with the choline cation. Its orientation, instead, is mainly determined by the Coulomb attraction of the carboxylate oxygen already engaged in the hydrogen bonding with choline (O_{A1} in Figure 2), giving origin to a weak,

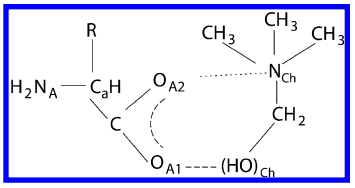

Figure 2. Schematic view of the [amino acid]$^-$ (left side)−[Chol]$^+$ (right side) docking geometry. R is the amino acid residue. The straight dashed line indicates a hydrogen bond, while the dotted line marks the close separation between the negatively charged O_{A2} atom on the anion side from the positively charged N_{Ch} atom of choline. The dashed circle represents the conjugation of the two CO_{A1} and CO_{A2} covalent bonds.

dx.doi.org/10.1021/jp412281n | J. Phys. Chem. B 2014, 118, 2471−2486

intraanion hydrogen bond O_{A1}—H—N_A that, in the [Chol]-[Ala] case is characterized by a fairly short O_{A1}—N_A separation ($d[O_{A1}-N_A]$ = 2.81 Å), but with a strained O_{A1}—H—N_A angle of only 101°. Additional OH, NH_2, or even SH functional groups on the residue R may donate a hydrogen bond to the primary amino group, which enhances the strength of the bond donated to O_{A1} in a remarkable manifestation of hydrogen bond cooperativity. In the [Chol][Ser] case, for instance, the O_{A1}—N_A separation is reduced to 2.67 Å, and the O_{A1}—H—N_A angle is now 113°. These features have been observed in isolated neutral ion pairs and may be significantly different in larger clusters or in extended systems.

Again in ion pairs, the amino acid residue (the R group in Figure 2) does not interact directly with the cation. In the case of neutral apolar residues such as the alkane tails of $[Ala]^-$ and $[Val]^-$, in particular, the residue interaction with $[Chol]^+$ is limited to relatively weak dispersion forces, whose magnitude increases with increasing size of the tail. A quantitative estimate of dispersion contributions to binding has been obtained by switching off the empirical (see Grimme[28]) corrections to our PBE+vdW functional. Without reoptimizing the geometry of either the separated or interacting ions, we find that dispersion forces contribute 6.6 kcal/mol to E_b of [Chol][Ala] and 7.0 kcal/mol in the case of [Chol][Val].

As already mentioned, the R residue plays a still secondary, but more significant, role in the case of the amino acids with additional functional groups, since they may form a somewhat strained hydrogen bond with the primary NH_2 amino group. More importantly, these groups represent additional polar centers interacting with the uneven charge distribution on $[Chol]^+$. Again in the [Chol][Ser] case, for instance, the distance of the hydroxyl oxygen of $[Ser]^+$ from the positively charged N_{Ch} on choline is fairly short (4.54 Å), pointing to a nonnegligible Coulomb interaction. Not surprisingly, similar observations hold in the case of [Chol][Cys], in which the OH group is replaced by SH. However, the longer S—H bond length and the lower polarity of the SH group with respect to OH decrease slightly the strength of the intraion hydrogen bond and increase the separation of S from the nitrogen atom on choline. These same features are instead enhanced in the case of [Chol][Asp], in which the additional COOH group of $[Asp]^+$ forms a strong intraion hydrogen bond with the amino group, while its other carboxylic oxygen points to nitrogen on choline, reaching a distance of 3.86 Å only from this atom. As we shall see in section IID, the hydrogen in the additional COOH group of $[Asp]^-$, which is known to be fairly acidic with a pK of 3.65, plays an important role in clusters and extended phases and could give rise to sizable proton conductivity.

The role of the R group in the aromatic systems that we analyzed such as [Chol][Phe] and [Chol][His] is more difficult to interpret and to describe in simple terms. In the case of [Chol][Phe], for instance, the residue seems to interact via polarization forces with choline and with the polar portion of the amino acid backbone, as shown by a sizable relaxation of the phenyl group upon separating or joining the two ions. Similar considerations apply to the [Chol][His] case, with the additional peculiarity that histidine comes in two varieties (see Figure 3), which in the literature often are described as *resonant*. In our computation the [Chol][His] ion pairs based on the two different $[His]^-$ isomers are indeed almost degenerate, with less than 2 kcal/mol difference in their total energy. The ground state of the ion pair is based on isomer a of Figure 3. The close balance of the two total energies, however,

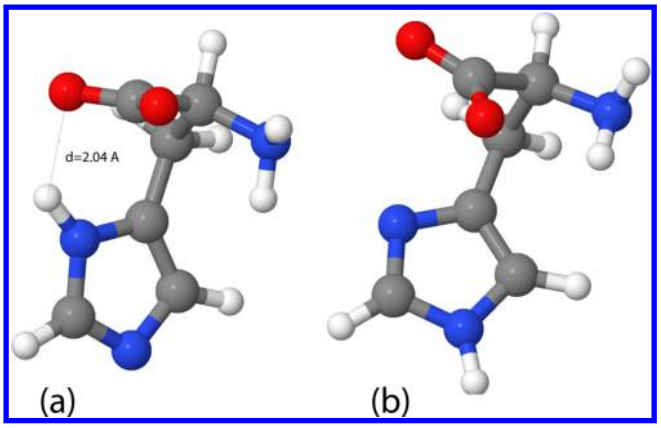

Figure 3. Resonant structures of the $[His]^-$ anion. In the gas phase, isomer a is 12 kcal/mol more stable than isomer b. The [Chol][His] ion pair based on isomer a is also more stable than the one based on isomer b, but its energy advantage is reduced to about 2 kcal/mol (see text).

hides sizable differences (~10 kcal/mol) in the energy of the building blocks. Gas-phase computations for the two $[His]^-$ isomers, in fact, show that isomer a is 12 kcal/mol more stable than isomer b, mainly because of the intraion hydrogen bond identified by the dashed line in part a of Figure 3. In the ion pair, however, this advantage is greatly reduced by the competition of this bond with the primary hydrogen bond joining the cation and the anion, which also explains the lower binding energy of [Chol][His] with respect to the other $[Chol]^+$ compounds. Even in these fairly bulky and highly polarizable anions, dispersion forces contribute only 7.4 kcal/mol to the [Chol][Phe] binding and 6.8 kcal/mol to that of [Chol][His].

More difficult is it to give a precise and unambiguous estimate of Coulomb and hydrogen bonding contributions to the total binding energy. For want of a better approach, we estimate the Coulomb contribution to the binding energy through the ESP charges, since the Hartree energy in the pseudopotential/plane wave calculations contain spurious terms arising from the valence—core interaction, and in the all-electron Gaussian computation it is dominated by the large contributions from the atomic cores. Taking this into account, the cation—anion Coulomb interaction energy is defined as

$$E_C = \sum_{i\in[cat]^+} \left\{ \sum_{j\in[an]^-} \frac{q_i q_j}{|\mathbf{R}_i - \mathbf{R}_j|} \right\} \quad (3)$$

where the $\{q_k\}$ are ESP charges, and $\{\mathbf{R}_k\}$ are the ground-state atomic positions. This definition, of course, neglects the relaxation of ions in their respective ground state, and, more importantly, it does not account for any variation of the ESP charges upon separation of the two ions. Nevertheless, E_C corresponds to the Coulomb interaction energy of a cation and anion pair in any force field adopting the set of ESP charges from our ab initio computation, and thus we use it here as a scale of ionicity in our systems. The results are in line with expectations. E_C overestimates the binding energy by 40—50%, accounting for the missing repulsive terms that fill the energy balance. According to this scale, [Chol][Ala] is the most ionic ion pair, whose E_C is 167.2 kcal/mol, while [Chol][Asp] is the least ionic one, with E_C = 136.7 kcal/mol. The full list of the E_C values is given in Table 3.

dx.doi.org/10.1021/jp412281n | J. Phys. Chem. B 2014, 118, 2471—2486

Table 3. Coulomb Interaction Energy, E_C, of Cation and Anion in the Ground State Ion Pairs, Computed According to Equation 3 (See Text)[a]

	$[Ala]^-$	$[Val]^-$	$[Ser]^-$	$[Cys]^-$	$[Asp]^-$	$[Asn]^-$	$[Phe]^-$	$[His]^-$
$[Chol]^+$	−167.2	−161.1	−143.0	−138.9	−136.7	−146.3	−161.3	−139.2
$[PhChol]^+$	−43.9		−47.3		−45.0			

[a]Energies per ion pair in kilocalories per mole.

It is worth mentioning that an equally plausible definition of E_C as the difference of Coulomb energy in the ion pair and in the isolated ions, thus including the relaxation of the ions as well as the change of the ESP charges upon their separation, gives unrealistically large E_C values, as well as large variations along the series of compounds, not reflecting the nearly constant binding pattern of the systems that we investigated.

Because of its directionality and short range, the hydrogen bond connecting O_{Ch} to O_{A1} is a primary factor determining the cation−anion docking geometry, even though the binding energy might be dominated by Coulomb contributions. The light proton, moving between the two oxygens by thermal energy and/or quantum zero point motion, might see a single minimum in the potential energy surface, corresponding to the actual equilibrium position, or it might find a secondary metastable energy basin, closer to the acceptor (O_{A1}) than to the donor (O_{Ch}) oxygen. Experimental and computational data[45] show that the energy surface has a single minimum when the equilibrium oxygen−oxygen distance $\bar{d}\{O-O\}$ is shorter that ≈2.75 Å, reverting to a double-well shape when $\bar{d}\{O-O\} >$ 2.75 Å . This picture can be quantified by computing the potential energy profile $\Delta E_{hb}(\zeta)$ (free energy profile, at nonzero temperature) seen by the proton moving along a reaction coordinate ζ joining the donor to the acceptor oxygen. Refined choices of the ζ coordinate have been proposed in the literature,[46] corresponding to a combination of all the geometrical parameters ($d\{O-O\}$, $d\{O-H\}$, $\theta\{O-H-O\}$) characterizing the bond. We make a simpler choice, defining ζ as the $H_{Ch}-O_{A1}$ distance. Decreasing ζ below the equilibrium $H_{Ch}-O_{A1}$ distance will force the proton to approach the acceptor oxygen, falling into the secondary energy minimum if this exists. To do so, we minimize again the system potential energy, with a constraint[38] on the value of the $\zeta = d\{H_{Ch}-O_{A1}\}$ distance. The $\Delta E_{hb}(\zeta)$ profiles obtained by our computations, shown in Figure 4 for [Chol][Ala] and [Chol][Asp], fully comply with the general picture of hydrogen bonding reported in the literature.[45] In all of the cases that we investigated, the $O_{Ch}-O_{A1}$ distance is shorter than $\bar{d}$, and the energy profile has a single minimum. The $d\{O_{Ch}-O_{A1}\}$ and $d\{O_{Ch}-H_{Ch}\}$ distances measured on the structures optimized under a constrained ζ are implicit functions of $d\{H_{Ch}-O_{A1}\}$. Their values, reported in the inset of Figure 4, allow one in principle to relabel the $\Delta E_{hb}(\zeta)$ plot according to different choices of the reaction coordinate and add structural detail on the changes in the hydrogen bond geometry upon changing the O_{A1}—H_{Ch} distance. For short elongation from the equilibrium distance, the motion along the generalized coordinate approximates the displacement pattern of the OH stretching mode, and the curvature of the potential around the minimum corresponds well with the frequency computed by diagonalizing the dynamical matrix. For longer distances, the constrained minimization along our reaction coordinate produces a more complex displacement pattern, mixing stretching and torsion modes, thus overemphasizing the anharmonicity of the potential well. It might be worth pointing out that the $O_{Ch}-$

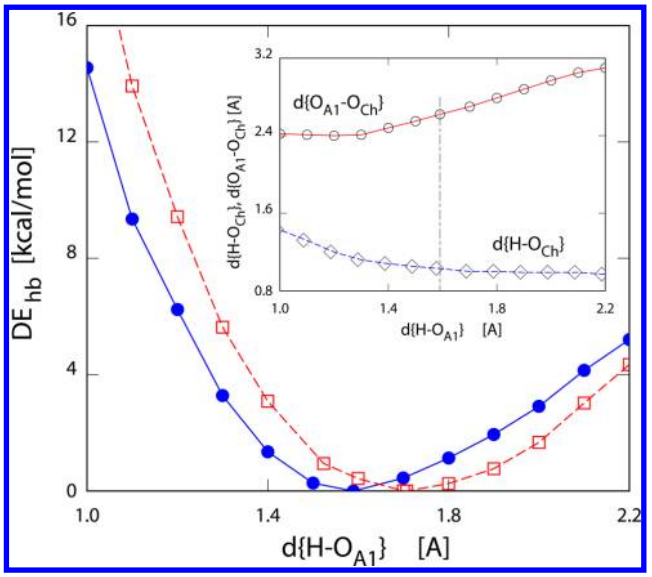

Figure 4. Potential energy of [Chol][Ala] (full dots, blue) and [Chol][Ser] (empty squares, red) as a function of the $H-O_{A1}$ distance, upon minimization with respect to all of the other coordinates. For each system, the zero of the energy corresponds to the ground-state energy of the ion pair. Lines are a guide to the eye. Inset: $O_{A1}-O_{Ch}$ (circles, red) and $H-O_{Ch}$ (diamonds, blue) distances in the minimum energy structure of [Chol][Ala] as a function of the constrained $H-O_{A1}$ distance. The equilibrium $H-O_{A1}$ separation in [Chol][Ala] is marked by the vertical dashed−dotted line.

H_{Ch} stretching mode has a zero point energy (zpe) of ∼4 kcal/mol and a first excitation energy of 8 kcal/mol, and thus even in its lowest lying states, the proton explores a wide range of ζ values, well beyond the strictly harmonic portion of the energy profile.

The electrostatic dipole of the ion pairs, ranging from the D = 4.8 D of [Chol][Asp], to the D = 15.2 D of [Chol][His] (see Table 4), is large when compared to the dipole of a prototypical polar molecule such as water, but small if we consider the fairly large size of the two ions. In fact, if we interpret these values in terms of two unit charges separated by a distance d, we obtain a very short estimate of their separation, ranging from d = 1 Å in the case of [Chol][Asp] to d = 3.2 Å for [Chol][His], in all cases shorter than the geometric size of the two ions. This effect is apparently due to the complementary polarity of the two ions, that arrange themselves in such a way to reduce the total dipole, thus minimizing the self-energy associated with the long-range dipolar electric field.

The ESP charges on atoms for all of the compounds that we analyzed are given as Supporting Information, and representative examples are shown in Table 5. Joining choline to its amino acid partner polarizes both species and enhances the charge on the atoms (N_{Ch}, O_{Ch}, H_{Ch}, O_{A1}, and O_{A2}) directly involved in the bonding with respect to the values computed for the gas-phase cations and anions. Remarkably, the amino group not directly in contact with choline retains the charge it has on the

dx.doi.org/10.1021/jp412281n | J. Phys. Chem. B 2014, 118, 2471−2486

Table 4. Dipole Moment (debye) of the Gas-Phase Neutral Ion Pairs

	$[Ala]^-$	$[Val]^-$	$[Ser]^-$	$[Cys]^-$	$[Asp]^-$	$[Asn]^-$	$[Phe]^-$	$[His]^-$
$[Chol]^+$	11.1	11.1	8.0	7.6	4.8	6.9	11.1	15.2
$[PhChol]^+$	10.8		11.5		15.1			

Table 5. Selected ESP Charges Computed on the Ground-State Structures of Neutral Ion Pairs and of Cations and Anions in the Gas Phase[a]

q_i/e	N_{Ch}	O_{Ch}	H_{Ch}	O_{A1}	O_{A2}	N_A
$[Chol]^+$	1.11	−0.65	0.44			
$[PhChol]^+$	1.00	−0.555	0.475			
$[Ala]^-$				−0.795	−0.83	−1.19
$[Ser]^-$				−0.81	−0.86	−1.045
$[Asp]^-$				−0.74	−0.75	−1.19
[Chol][Ala]	1.51	−0.79	0.63	−0.84	−0.98	−1.07
[Chol][Ser]	1.425	−0.75	0.58	−0.80	−0.91	−1.06
[Chol][Asp]	1.26	−0.72	0.54	−0.75	−0.80	−1.18
[PhChol][Ala]	1.23	−0.81	0.59	−0.69	−0.82	−0.98
[PhChol][Ser]	1.18	−0.82	0.61	−0.69	−0.80	−1.025
[PhChol][Asp]	1.15	−0.99	0.57	−0.66	−0.78	−0.99

[a]PBE+vdW approximation for the exchange-correlation energy. The naming of atoms follows Figure 2. The full set of atomic charges is given as Supporting Information.

Table 6. Comparison of Binding Energies Computed by GGA(PBE+vdW)/Plane Waves (Upper Line) and Hybrid (M06-2X +vdW) Functional/Gaussian Basis (Lower Line)[a]

	$[Ala]^-$	$[Val]^-$	$[Ser]^-$	$[Cys]^-$	$[Asp]^-$	$[Asn]^-$	$[Phe]^-$	$[His]^-$
$[Chol]^+$	106.0	104.6	104.9	104.6	102.7	104.9	102.7	93.3
	106.0	104.8	106.5	106.0	105.0	106.8	104.0	94.5
$[PhChol]^+$	113.8		110.2		103.2			
	118.8		108.7		116.2			

[a]All energies in kilocalories per mole per ion pair.

Table 7. Comparison of Selected Structural Parameters in $[Chol]^+$ Compounds Computed by GGA(PBE+vdW) /Plane Waves (Upper Line of Each Item) and Hybrid (M06-2X+vdW) Functional/Gaussian Basis (Lower Line)[a]

	$[Ala]^-$	$[Val]^-$	$[Ser]^-$	$[Cys]^-$	$[Asp]^-$	$[Asn]^-$	$[Phe]^-$	$[His]^-$
$O_{a1}-O_{Ch}$	2.62	2.62	2.65	2.66	2.70	2.66	2.62	2.65
	2.68	2.68	2.70	2.70	2.74	2.72	2.69	2.70
$O_{A1}-H-O_{Ch}$	179	179	173	170	168	175	177	173
	166	166	163	165	166	166	165	162
$O_{A1}-N_{Ch}$	3.28	3.30	3.36	3.44	3.45	3.34	3.29	3.35
	3.28	3.28	3.34	3.33	3.41	3.36	3.32	3.36

[a]Distances are in angstroms and angles in degrees.

corresponding amino acid anion. Surprisingly, this effect seems to affect slightly more the cation than the anion, which could have been expected to be more polarizable. We do not have an explanation of this observation, but while the enhanced polarity of both species is clearly confirmed in all systems, the different behavior of cation and anion is perhaps within the error bar of the somewhat uncertain ESP method.

Binding energy and geometrical parameters characterizing the cation−anion bonding computed by M06-2X/D3 are compared to their PBE+vdW counterpart in Table 6 and Table 7. It is apparent that the binding energies obtained by the two methods agree remarkably well, with relative differences of the order of 1%. Interatomic distances and angles display slight but systematic differences, as M06-2X/D3 overestimates the $O_{Ch}-O_{A1}$ distance by about 2% and the $O_{Ch}-H-O_{A1}$ angle is underestimated by up to 12° with respect to the PBE+vdW result. The $N_{Ch}-O_{A2}$ distance, on the other hand, shows again good agreement between the two methods.

The atomic charges computed by the NBO analysis on the M06-2X/D3 ground-state orbitals are also remarkably close to those provided by the ESP method used in the PBE+vdW/plane wave computations. As already mentioned in section II, this is remarkable since the two methods differ significantly in their approach to the problem, and their good agreement supports the reliability of both sets of charges to represent Coulomb interactions in our molecules.

The NBO analysis of the M06-2X/D3 Kohn−Sham orbitals provides also a scale to compare the strength of the hydrogen bonds in the compounds that we investigated. The data for the cation−anion hydrogen bond, as expected, faithfully reflect the geometrical parameters, and follow, in particular, the $O_{Ch}-O_{A1}$ distance. The absolute value of the NBO H-bond parameter, ranging from 18.9 kcal/mol for [Chol][Asp] to 24.5 kcal/mol for [Cho][Ala], appears to overestimate the energy of hydrogen bonds of comparable oxygen−oxygen distance in other compounds,[45] but the interpretation of the NBO energy

dx.doi.org/10.1021/jp412281n | J. Phys. Chem. B 2014, 118, 2471−2486

parameter has to take into account the considerations listed in section II. The relative scale provided by this parameter, however, shows that the apparent intraanion hydrogen bonds in [Chol][Ser], [Chol][Cys], and [Chol][Asn] are weak, while the one in [Chol][Asp] is much stronger than the anion−cation hydrogen bond through O_{Ch}−O_{A1}, consistently with the recognized acidic character of the proton in the second carboxylic -COOH group of $[Asp]^-$.

As a further check, the ground-state geometry of [Chol][Ala] has been reoptimized at the MP2/6-311+G(d) level. The MP2 and the M06-2X/D3 geometries are indeed very similar, with a mean square difference between the two structures of only 0.22 Å. The O_{Ch}−O_{A1} distance, for instance, changes from 2.68 to 2.70 Å when moving from M02-2X/D3 to MP2, while the O_{A1}−N_{Ch} distance changes from 3.29 to 3.30 Å. Given the similarity of the PBE+vdW and M06-2X/D3 results, the conclusions of this comparison can be extended directly to PBE.

B. Vibrational Properties. Vibrational properties in the harmonic approximation of the PBE+vdW model have been determined by diagonalization of the dynamical matrix computed by finite differences. The density of states (DOS) given by our computations is similar to that of many organic systems of comparable chemical composition, characterized by a high-frequency ($\geq$2800 cm^{-1}) band due to the stretching of covalent Y−H bonds (with Y being C, ,N or O), possibly broadened by hydrogen bonding, an intermediate-frequency ($1400 \leq \omega \leq 1600$ cm^{-1}) band due to H−Y−H bending modes, and a broad background extending up to 1400 cm^{-1} of mixed modes, accounting for the stretching and bending of bonds involving elements heavier than H, torsion, and rotations of submolecular molecular groups.

The most apparent effect of the ion pairing is the drastic lowering of the stretching frequency of the OH group giving rise to the hydrogen bond connecting the cation and the anion. The large red shift, of the order of 600 cm^{-1} and up to 900 cm^{-1}, is consistent with the high strength of this bond, as confirmed also by the short distance separating the two oxygen atoms on choline and on the amino acid (see Table 2). Because of this shift, in all cases the stretching of this special hydroxyl group is located at the low-energy side of the high-frequency band accounting for the stretching of all covalent bonds involving hydrogen.

Apart from this easily predictable change, the DOS of each ion pair is almost exactly the sum of the contributions computed for the two isolated ions. Moreover, the vibrational DOSs of all of these compounds are fairly similar, apart from a different normalization due to the different system sizes, as can be appreciated in Figure 5, comparing the DOSs computed for [Chol][Ala], [Chol][Phe], and [Chol][His].

A closer examination of the computational results, however, highlights a number of features that could assist in the interpretation of the experimental data. In all ion pairs, for instance, the highest frequency eigenstates correspond to the N−H stretching modes of the NH_2 group (or groups, in the asparagine case), slightly split by their mutual interaction. The formation of intraanion hydrogen bonds in the serine, cysteine, and aspartic acid cases, in which NH_2 acts as the acceptor, increases slightly both the frequency and the splitting of these modes.

The first modes below the highest frequency band, found at ~1600 cm^{-1} and localized again on the amino group, correspond to the H−N−H bending, somewhat mixed with

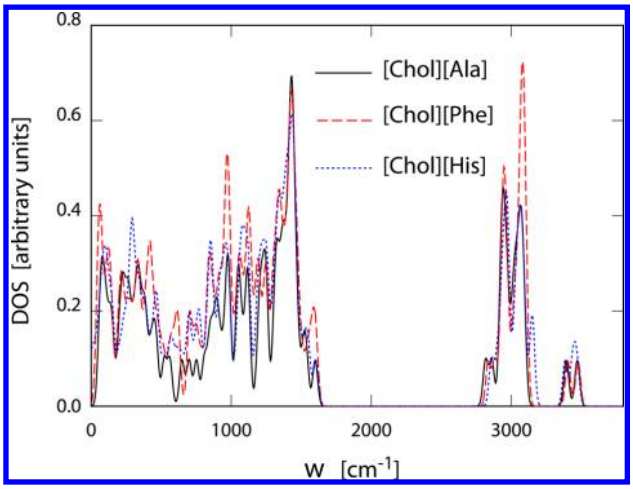

Figure 5. Comparison of the vibrational density of states computed for [Chol][Ala] (full line, red), [Chol][Phe] (dashed line, blue), and [Chol][His] (dotted line, black). Discrete energy eigenvalues have been broadened by convolution with a Gaussian of 12 cm^{-1} width. The area under each curve is equal to the number of modes of the corresponding ion pair.

the stretching of covalent bonds in the carboxylate group(s) of each amino acid. A comparable frequency is computed also for the bending of the COH apex of choline, moving the hydrogen out of the H-bond direction.

This information on vibrational eigenstates involving hydrogen, and focused on medium-high frequency modes, could be of interest for instance, in designing inelastic and quasi-elastic neutron scattering experiments that are especially sensitive to proton dynamics. Most experimental studies of vibrational properties, however, rely on infrared and Raman spectroscopy, and often target modes at low and medium energies (up to ~1600 cm^{-1}), which arguably are the most interesting ones to probe complex intermolecular (interion, in this case) interactions.

Our computations give us an easy access to the infrared activity of the gas-phase ion pairs. The results are shown in Figure 6. The first observation is that the infrared matrix

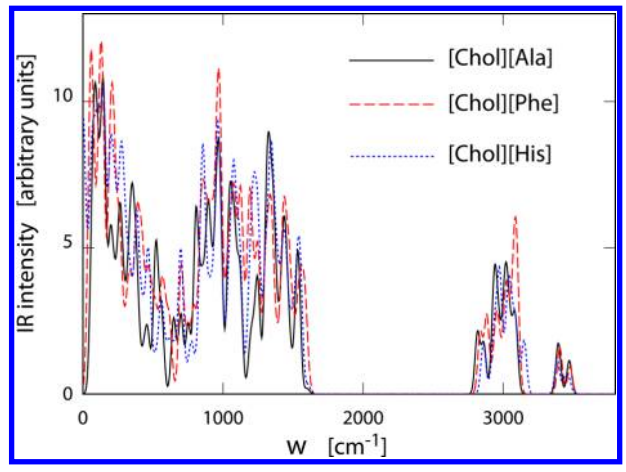

Figure 6. Infrared activity of [Chol][Ala] (full line, red), [Chol][Phe] (dash line, blue), and [Chol][His] (dotted line, black). The three curves are normalized in such a way that the underlying vibrational DOS (i.e., without the IR weight) integrates to the number of modes of the corresponding ion pair.

dx.doi.org/10.1021/jp412281n | J. Phys. Chem. B 2014, 118, 2471−2486

Table 8. Lowest Energy Singlet and Triplet Electron Excitation Energies of Ion Pairs Consisting of the Choline Cation and an Amino Acid Anion[a]

	$[Ala]^-$	$[Val]^-$	$[Ser]^-$	$[Cys]^-$	$[Asp]^-$	$[Asn]^-$	$[Phe]^-$	$[His]^-$
				$[Chol]^+$				
$\Delta S = 0$	4.75	4.72	5.35	4.80	5.23	4.92	4.58	4.47
	(3.68)	(3.69)	(4.04)	(3.85)	(4.29)	(4.03)	(3.62)	(3.85)
$\Delta S = 1$	4.18	4.20	4.63	4.56	4.77	4.45	3.93	4.01
	(3.11)	(3.11)	(3.47)	(3.37)	(3.66)	(3.51)	(3.14)	(3.51)
				$[PhChol]^+$				
$\Delta S = 0$	5.12		5.13		5.10			
$\Delta S = 1$	4.34		4.38		4.40			

[a]The excitation energies of the corresponding gas-phase amino acid anion are shown in parentheses. Energies in electronvolts.

elements enhance the relative weight of the low-frequency modes. Because of the low symmetry of the system, almost all modes carry at least a small portion of IR activity, and, especially for the low-frequency vibrations, often it is difficult to give a simple interpretation of the corresponding displacement pattern. A few peaks at ∼150−180 cm^{-1}, 350−400 cm^{-1}, and ∼700−800 cm^{-1}, however, stand out of the background and are present in all of the choline-based ion pairs. Not surprisingly, they all correspond to modes affecting the relative position of the most charged functional groups. The lowest energy ones, up to 400 cm^{-1}, in particular, correspond to the stretching and shearing of the $O_{Ch}-O_{A1}$ and $N_{Ch}-O_{A2}$ distances. It is tempting to consider them as the precursors of the (Γ-point) optical modes in hypothetical crystal phases of these compounds. Vibrational eigenvectors are given as Supporting Information.

The zpe amounts to 179 kcal/mol in [Chol][Ala] and 228 kcal/mol in [Chol][Phe]. Including zpe in the total energy of all species decreases the cation−anion binding energy by a few kilocalories per mole. In other words, the zero point energy of the neutral pair is 1 or 2 kcal/mol higher than the sum of the two isolated ion contributions (see Table 1). The small size of this effect apparently reflects the near additivity of the vibrational spectra already pointed out in the previous paragraphs and seems at odds with the large downward shift of the high-frequency stretching modes localized on the atoms at the cation−anion close contact region. It would be tempting to attribute this systematic trend to the decrease in the number of modes of vanishing frequency from 6 + 6 for the separate ions to only 6 in the ion pair case. A closer analysis of the variations in vibrational eigenvalues and eigenvectors upon ion pairing, however, reveals a complex pattern or compensations among different modes, whose net result is difficult to predict without an explicit computation of the frequency of all modes.

Vibrational properties computed at the M06-2X/D3 level of approximation agree qualitatively with the PBE+vdW results, but their frequencies are systematically ∼10% higher. At first sight, the PBE+vdW predictions seem closer than M06-2X/D3 to experimental data on peptides and proteins,[47] spanning fairly accurately the same frequency range. Moreover, and perhaps more importantly, the PBE+vdW frequency of characteristic modes such as stretching and bending of easily identifiable groups agrees well with spectroscopic data on simpler systems. However, even neglecting the effect of the solvent, which is present in experiments and absent in the computations, the interpretation of this simple observation is less than straightforward. Irrespective of the functional, our computations provide strictly harmonic frequencies, while in reality all modes are affected by nonnegligible anharmonicity that, in general, tends to decrease their frequency. This fact is recognized by the computational quantum chemistry community and pragmatically corrected through an empirical scaling factor (<1). Thus, the present state of the art offers the choice between a method (PBE+vdW) whose good agreement with experiments might arise from a fortuitous cancellation of errors, and a more CPU intensive approach whose predictions need to be scaled by an ad-hoc number. For completeness, we mention that for M06-2X/D3 the suggested value of the rescaling factor is 0.94.[30]

C. Excitation Energies by ΔSCF Computations. The ionic bond is typically associated with an electronic insulating character of the compound, and, in this respect, organic ionic liquids are no exception. Most RTIL's, in fact, are transparent, but peculiar and potentially interesting optical properties have been discussed in the literature.[48] A detailed investigation of optical properties is beyond the scope of the present study. However, as a first exploration of excited-state properties of RTILs by computational means, we estimated the fundamental optical gap by the ΔSCF approach.

The results of our computations are summarized in Table 8. Their interpretation relies on the comparison with the excitation energies of cation and anion isolated in the gas phase, computed by the same ΔSCF method. As mentioned in the introductory part of section III, the two cations are highly insulating, with a vertical gap for the singlet excitation of 8.06 eV (choline) and 6.80 eV (phosphocholine). The amino acid moieties, on the other hand, display lower gaps, consistent with their anionic character, giving them a more polarizable electronic configuration. From these observations, it is natural to expect the excitation energy of the ion pairs to be intermediate between those of the cation and anion, and closer to the latter. This expectation is borne out by the ΔSCF results shown in Table 8 and in Figure 7, confirming that in the [Chol][amino acid] compounds the excitation energy of the pairs reflect primarily those of the corresponding amino acid anion. This, in turn, suggests that the excitation is predominantly localized on the anion, with the cation representing a barrier for the excited-state orbitals, increasing its energy by about 1 eV. Again as expected, the lowest excitation energies are computed for the amino acids with aromatic residues such as [Chol][Phe] and [Chol][His], the highest for the least polarizable species such as [Chol][Asp] and [Chol][Ser]. In agreement with the results of ref 49, and at variance from earlier conjectures, no obvious correlation is found between the fundamental gap of the anions and the strength of the hydrogen bond linking the ion pairs, nor with the hydrogen binding propensity of the resulting neutral molecules.

dx.doi.org/10.1021/jp412281n | J. Phys. Chem. B 2014, 118, 2471−2486

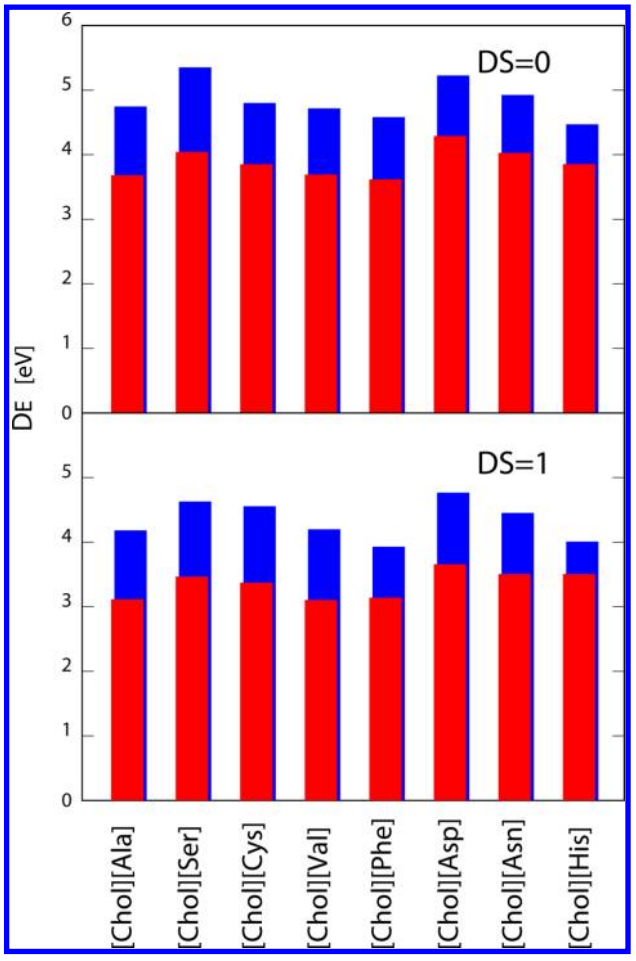

Figure 7. Singlet ($\Delta S = 0$) and triplet ($\Delta S = 1$) vertical excitation energies for the neutral ion pairs (blue histogram) and for the corresponding gas-phase anions (red histogram). Computations have been carried out using the ΔSCF approach (see section II) with the PBE+vdW approximation for the exchange-correlation energy.

In all cases, the computed optical ($\Delta S = 0$) gap corresponds to absorption in the near-ultraviolet (UV) range. Triplet excitation energies are systematically lower than the corresponding singlet energies by about 0.6 eV, still remaining in the near-UV range. In this respect, the optical properties of these systems are similar to those of proteins,[50] also comparable to those measured on other RTILs based on imidazolium.[48]

We did not compute dipole matrix elements between the ground and the excited orbitals, and therefore we do not know the oscillator strength of the singlet excitations.[51] However, given the complex and irregular shape of these molecular species, it is very unlikely that the lowest energy excitations determined in our computations are suppressed by symmetry.

D. Molecular Dynamics Simulations for Small Clusters. Ab initio molecular dynamics simulations of small neutral clusters have been carried out for the simplest of the ionic compounds considered in the previous sections, i.e., [Chol]-[Ala], and for [Chol][Asp], whose acidic protons give rise to a variety of isomers interconnected by the transfer of protons among electronegative functional groups.

More precisely, we simulated [Chol][Ala] clusters made of one, two, and four ion pairs, and [Chol][Asp] clusters made of one and three ion pairs. Simulations have been carried out in the microcanonical (NVE) ensemble by CPMD, using the same plane wave and exchange-correlation setting of the ground-state computations described in the previous sections. The temperatures listed in subsequent text have been computed from the average kinetic energy of atoms along the simulation trajectory and have been set by velocity rescaling (see Berendsen et al.[52]) during the equilibration stage. The error bar is estimated by the standard error of T averaged on subblocks of 1000 steps.

The $\{[Chol][Ala]\}_n$ (n = 1, 2, 4) simulations mainly confirm the stability of individual ion pairs identified by their hydrogen bond connection and highlight even further the importance of polar interaction in addition to the bare Coulomb ones.

Simulations for the single ion pair at $T = 156 \pm 5$ K, for instance, show the expected combination of stretching, bending, and torsion of covalent bonds. More interestingly, they also show relatively regular oscillations of the $O_{Ch}-O_{A1}$ and $N_{Ch}-O_{A2}$ distances. In the $O_{Ch}-O_{A1}$ case, these oscillations are low amplitude, relatively fast, and fairly harmonic, giving rise to the characteristic double-horn probability distribution for this distance shown by the black line in Figure 8. In the $N_{Ch}-O_{A2}$ case, the motion is slower, it

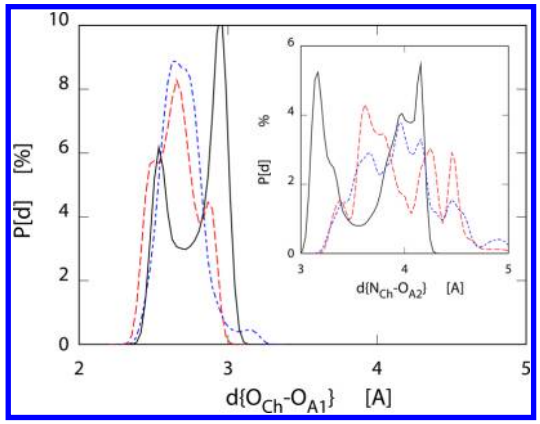

Figure 8. Probability distribution[53] of the $O_{Ch}-O_{A1}$ distance in $\{[Chol][Ala]\}n$ clusters, n = 1 (black line), n = 2 (red dashed line), and n = 4 (blue dotted line), at T = 150 K. Inset: same plot for the $N_{Ch}-O_{A2}$ distance.

spans a wider range, and the slight anharmonicity of the underlying potential splits one of the peaks in the probability distribution, as can be seen in the inset of Figure 8.

Simulations for $\{[Chol][Ala]\}_2$ show that the two ion pairs arrange themselves on a square checkerboard geometry, in such a way that their Coulomb interaction is optimized, while the relative orientation of the ions is such that it effectively cancels the total dipole moment of the cluster. The lowest energy structure found by simulated annealing is shown in Figure 9 and has a total dipole moment of less that 1.8 D, comparable to the dipole moment of a single water molecule. Within each ion pair, the hydrogen bond connecting the hydroxyl termination of $[Chol]^+$ to the O_{A1} oxygen of $[Ala]^-$ appears to be as strong and nearly as short as in the isolated ion pair case, thus effectively identifying individual ion pairs. The partner O_{A2} oxygen, instead, is nearly equidistant from the nitrogen atoms on the two $[Chol]^+$ units, thus providing the link between the two ion pairs.

The cohesive energy of $\{[Chol][Ala]\}_2$ with respect to two separated [Chol][Ala] units is 0.83 eV (total) or 9.6 kcal/mol per ion pair. In other terms, the cohesive energy of each [Chol][Ala] pair is 1 order of magnitude smaller than the cation−anion binding energy within the pair.

dx.doi.org/10.1021/jp412281n | J. Phys. Chem. B 2014, 118, 2471−2486

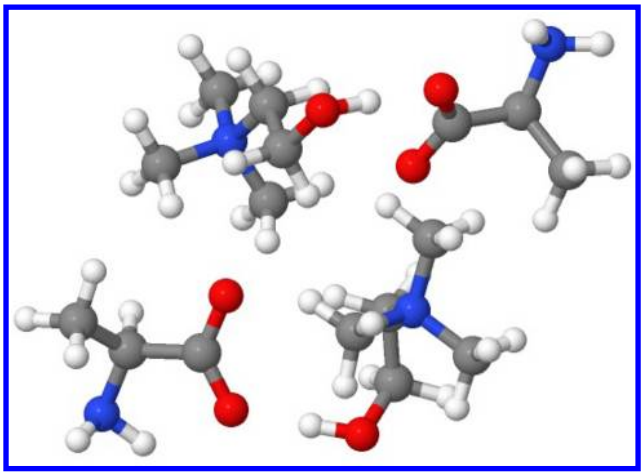

Figure 9. Ground-state structure of $\{[Chol][Ala]\}_2$.

Raising the temperature to $T = 153 \pm 4$ K in an NVE simulation does not change significantly the ground-state picture. The hydrogen bonds, and thus the ion pair identity, remain well-defined, as highlighted by the narrow probability distribution[53] for the $O_{Ch}-O_{A1}$ distances (see Figure 8). The corresponding probability distribution for the $O_{A2}-N_{Ch}$ distance is broader, reflecting the longer range and softer restoring force of this electrostatic bond, and less regular, because of the multiple interactions resulting from the sharing of O_{A2} between the nitrogen atoms on the two choline cations (see again Figure 8). Admittedly, our simulations (6 ps after equilibration) are too short to provide evidence of a longer time scale dynamics of the hydrogen bonds, but the narrow probability distribution of the $O_{Ch}-O_{A1}$ distance is a clear indication of the strength and stability of the ion pair molecular unit. Because of the relatively low cohesion between the two ion pairs, we did not explore a wider temperature range.

The simulations for $\{[Chol][Ala]\}_4$ again at $T = 148 \pm 3$ K mainly confirm the picture provided by the $\{[Chol][Ala]\}_2$ case. In particular, they underline the stability of the [Chol][Ala] ion pairs, none of which interchanges partners during our 6 ps production run following equilibration. Moreover, the simulation trajectories confirm the relatively inert character of the NH_2 termination of $[Ala]^+$, in the absence of additional functional groups in the amino acid residue R. Polymer-like configurations consisting of alternating cations and anions stretching all the way across the simulation cell appear often in the simulation and highlight the role of dipolar forces at low temperature.[54]

Annealing the $\{[Chol][Ala]\}_4$ cluster produces a few distinct low-energy structures. The lowest energy one can be described as an ellipsoidal loop of alternating cations and anions, once again of nearly vanishing dipole moment. The cohesive energy of this structure with respect to the four separated ion pairs is 2.85 eV (total), or 16.4 kcal/mol per ion pair.

From experimental measurements[18] we know that the density of these liquids is about 1.05 g/cm^3. Together with the known molecular weight, this information allows us to assign a volume, and thus a radius and a surface area, to each cluster, approximating the cluster shape by a sphere and assuming that the density remains unchanged down to the molecular limit.

If R_1 is the radius of the neutral ion pair, the radius R_N and surface area S_N of an N-pair cluster will be

$$R_N = N^{1/3} R_1 \tag{4}$$

$$S_N = N^{2/3} S_1 = 4\pi N^{2/3} {R_1}^2 \tag{5}$$

The simplest definition of the surface energy is

$$\frac{E(N)}{N} = \epsilon(\infty) - \gamma \frac{S_1}{N^{1/3}} \tag{6}$$

where $E(N)$ is the cohesive energy of the N-pair cluster with respect to the isolated pairs and $\epsilon(\infty)$ is the limit of $E(N)/N$, $N \to \infty$. In this equation, $E(N)$ and S_1 are known, while $\epsilon(\infty)$ and γ are unknown. We use the $E(N)$ values for $N = 2$ and $N = 4$ computed for [Chol][Ala] to obtain both $\epsilon(\infty) = 42.6$ kcal/mol, and $\gamma = 132$ mJ/m^2. Admittedly, this is only a very approximate estimate of these two quantities, since we neglect a number of effects such as the density variation with decreasing system size caused by the Laplace pressure, the curvature (and thus size) dependence of the surface energy, and also the fact that small clusters are certainly nonspherical, and the surface energy is nonuniform across the cluster surface. However, the fairly high cohesive energy per ion pair ($\epsilon(\infty)$) predicted for homogeneous phases supports the ionic character of these compounds, and the estimate of the surface energy, much higher than typical values measured in neutral organic systems and close to the experimental and computational data for imidazolium-based ionic liquids,[55] provides a further check of the ionic compound picture.

The results for [Chol][Asp] are more intriguing, since even in the short time allowed by ab initio simulation, we observe several events of proton transfer. These concern primarily the acidic proton on the secondary $COOH^-$ group of $[Asp]^-$, which in the ground-state structure of [Chol][Asp] gives rise to a hydrogen bond with the amino group. More precisely, a first NVE simulation of $\{[Chol][Asp]\}_3$ at $T = 150$ K reproduces once again the picture seen in the [Chol][Ala] clusters at the same temperature, the only noticeable difference being the relatively low-frequency, large-amplitude oscillations of the proton in the secondary -$COOH^-$ group, making occasional jumps to the primary amino group. Raising the temperature to $T = 200$ K triggers a sequence of events that in our short simulations appear to be related. First of all, the -$COOH^-$ proton spends nearly half of its time on the amino group, which then donates another one of its protons to the carboxylate group of another anion. The increased average separation of the $O_{Ch}-O_{A1}$ atoms in the primary hydrogen bond gives it a double-well character, and the proton in between spends ~25% of its time closer to O_{A1} than to the original O_{Ch} atom. All of these changes blur the neat ionic picture of [Chol][Asp] and provide a variety of proton-transfer mechanisms, which, in turn, could make [Chol][Asp] a promising proton conductor, provided suitable paths could be found for the long-range diffusion of protons.

Admittedly, the sample is too small and the simulation is too short to investigate in detail proton conductivity issues. Moreover, the picture could be even more complex in the presence of a solvent such as water that provides an additional and abundant proton reservoir. Further experimental and computational studies will be needed for a reliable assessment of the proton conductivity of [Chol][Asp] and similar compounds in their liquid phases.

dx.doi.org/10.1021/jp412281n | J. Phys. Chem. B 2014, 118, 2471−2486

IV. REPLACING CHOLINE WITH PHOSPHOCHOLINE

As already noted, the docking site provided by the phosphocholine cation ($[PhChol]^+$) to incoming amino acid anions is similar to that of choline, and the moderate increase (from 3.01 Å in $[Chol]^+$ to 4.36 Å in $[PhChol]^+$) of the nitrogen−hydroxyl distance on $[PhChol]^+$ is to some extent compensated by the enhanced flexibility of the cation, due to rotation and bending degrees of freedom the H_2PO_4 group added to the choline structure. As a result, the distance and relative orientation of the anion carboxylate from the hydroxyl group and positively charged cation's nitrogen are nearly the same in the choline and phosphocholine cases, as shown in Table 2.

Despite the geometric similarity, the replacement of the choline cation with its phosphocholine counterpart qualitatively changes the binding character of these compounds, since, upon formation of the hydrogen bond between the cation and anion, in all three cases that we considered, the shared proton moves from phosphocholine to the amino acid side, effectively neutralizing both species. This change, apparently due to the different p*K*s of choline and phosphocholine, drives an ionic to polar transition, giving origin to a neutral but highly polar material made of two molecular species. The transition, however, corresponding to only a short-range displacement of the H-bond proton, cannot affect drastically the geometry, the binding energy, and so on of the resulting pair of molecules. Binding energies, computed again with respect to the gas-phase ions are even (slightly) higher than those of the choline compounds, due to a parallel enhancement of dispersion and polar interactions. To be precise, the moderate increase of binding energy that we compute is the net result of several competing interactions, such as the slight enhancement of hydrogen bonding revealed by the shrinking of the $O_{Ph}-O_{A1}$ distance, and the equally moderate reduction of Coulomb attraction between $N_{Ch}-O_{A2}$, whose distance increases slightly. Dispersion interactions contribute 5.8, 6.4, and 6.0 kcal/mol to the binding energy of [PhChol][Ala], [PhChol][Ser], and [PhChol][Asp], respectively.

ESP charges have been computed on the ground-state structures, and the results are reported in Table 5. The first observation is that the atomic charges of the phosphocholine compounds are relatively close to their choline counterparts. A more quantitative analysis shows that the phosphocholine nitrogen is slightly ($|\Delta q_N| \sim 0.2e$) but systematically less positively charged than in the choline compounds, perhaps because of the increased distance and lower polarization from the O_{A2} atom. The trend toward reduced ionicity in the [PhChol][Amin] molecules, in fact, is fairly general and perhaps is due to the screening effect of the polarizable H_2PO_4 group. Apart from the cation nitrogen case, however, the variation of atomic charges between choline and phosphocholine compounds is ∼0.02*e*, i.e., 1 order of magnitude less than for nitrogen. Finally, the interchange of donor/acceptor role between the phosphocholine oxygen and O_{A1} is accompanied by the systematic variation in their charge: while in the choline compounds, O_{A1} is always more negative than its partner on the cation side, the opposite is true in the corresponding phospholipid cases. All of the computed charges are provided as Supporting Information.

Remarkably, the change of binding character from ionic to strictly polar is reflected in a drastic drop of the parameter E_C computed according to eq 3, as shown in Table 3, supporting the interpretation of E_C as a measure of ionicity.

The most obvious changes in vibrational properties concern again the highest frequency modes. Phosphocholine has two hydroxyl terminations instead of the single one of choline, and the highest frequency mode in isolated [PhChol][Amin] molecules is the stretching of the lone OH group remaining on $[PhChol]^+$ after the transfer of the other terminal proton to the amino acid. The very strong hydrogen bond joining the O_{A1} donor to the O_{PhChol} acceptor is reflected into an unusually large softening of the $O_{A1}-H$ stretching mode, whose frequency turns out to be $\omega \sim 2400$ cm^{-1}, i.e., in the middle of the gap separating bending modes from the high-frequency band of Y−H (Y being C, N, or O) stretching.

Most other features are the same in the choline and phosphocholine cases. In particular, the DOS of the combined molecule is nearly the sum of those of the isolated ions, and the major difference between the choline and the phosphocholine cases is represented by a bunch of modes at low and medium frequency, accounting for the rotations and bending and stretching modes of the H_2PO_4 group. The prominent features in the spectra of infrared activity seen in the choline compounds are still present, but more fragmented and less apparent than in the choline compounds, apparently because of the additional centers of Coulomb interaction represented by the highly charged atoms in the H_2PO_4 group. Moreover, the infrared activity of the $[PhChol]^+$ compounds is globally less intense than in the corresponding $[Chol]^+$ systems (see Figure 10), perhaps reflecting the neutrality of the two molecular moieties. Vibrational eigenvectors and infrared activity are given as Supporting Information.

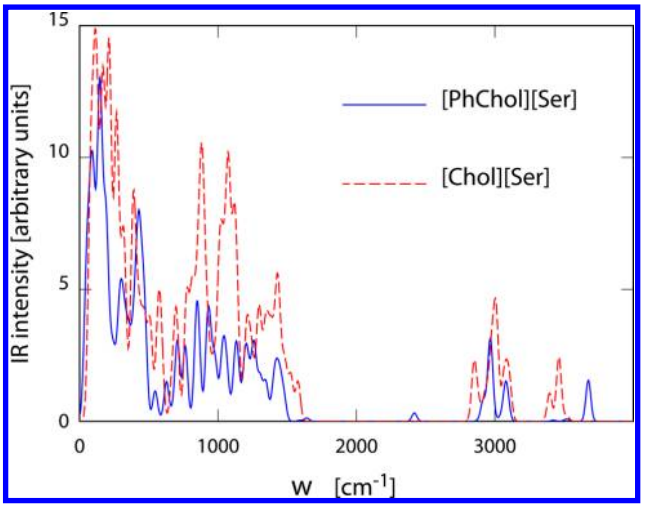

Figure 10. Comparison of the infrared activity of [PhChol][Ser] (full curve, blue) and of [Chol][Ser] (dashed curve, red). The area under each curve is normalized as in Figure 6

The energy profile seen by the proton along the ζ coordinate joining O_{A1} to O_{PhChol} is similar to the one computed for the $[Chol]^+$ compounds, once the interchange of the donor and acceptor role of the two oxygen atoms is taken into account. The curvature of $\Delta(\zeta)$ at the equilibrium distance is less than in the previous case, consistently with the further drastic softening of the OH stretching mode down to $\omega \sim 2400$ cm^{-1}.

Replacing $[Chol]^+$ with $[PhChol]^+$ affects only slightly excitation energies, with differences from the choline case that are not systematic. The first interesting observation, perhaps, is that excitation energies are almost the same for

dx.doi.org/10.1021/jp412281n | J. Phys. Chem. B 2014, 118, 2471−2486

[PhChol][Ala], [PhChol][Ser], and [PhChol][Asp] and thus, at variance from the choline case, do not reflect the ordering of excitation energies in the corresponding amino acids. This, in turn, suggests that excited-state orbitals are no longer confined on the anion, but extend toward the cation, probably because of its enhanced polarizability. The insensitivity of the excitation energies on the amino acid choice, in particular, points to a localization of the excited-state orbitals on the contact area between the two ions, which remains remarkably conserved along the amino acid sequence. Also in the phosphocholine case, all excitation energies are in the near-ultraviolet portion of the spectrum.

V. SUMMARY AND CONCLUSION

First principle computations based on semilocal (PBE+vdW) and hybrid (M06-2X/D3) exchange-correlation approximations have been carried out for a series of neutral organic ion pairs consisting of a $[Chol]^+$ or $[PhChol]^+$ cation coupled to a deprotonated amino acid anion (see Figure 1).

Simulated annealing and GEDIIS[33] geometry optimization for the $[Chol]^+$ compounds reveal a characteristic docking geometry of the two ions, schematically illustrated in Figure 2. The conservation of this same geometry with very similar interatomic distances along the series of compounds that we considered, i.e., [Chol][Ala], [Chol][Ser], [Chol][Cys], [Chol][Val], [Chol][Phe], [Chol][Asp], [Chol][Asp], and [Chol][His], reflects the dominant role of a strong and short hydrogen bond joining cation and anion through the $O_{Ch}-H_{Ch}$ and O_{A1} atoms, as well as the Coulomb attraction of the positively charged nitrogen on $[Chol]^+$ on the O_{A2} oxygen on the amino acid side. The detailed analysis of geometries and charge distribution highlights the complementary but still important role of polar interactions in addition to the bare Coulomb ones, boosting the cohesive energy E_b of each neutral molecule to more than 100 kcal/mol per pair. The role of polar forces is further emphasized by the low dipole moment of the ion pairs, pointing to the energetic imperative of reducing as far as possible the intensity and range of the electrostatic fields arising from the molecule. Dispersion (van der Waals) interactions, estimated through an empirical correction to the DFT functionals, contribute about 5% to E_b, and vibrational terms contribute even less (~2% of E_b). The amino group and additional functional groups (OH, NH_2, and SH) in the amino acid residue R do not interact directly in the ion pairs, but are likely to play a more active role in larger aggregates.

Gaussian09 computations based on hybrid functionals confirm the PBE+vdW results for energies and geometries, and enhance our confidence in the validity of the picture emerging from our study. Cation−anion binding energies, in particular, agree to about 1%, while the geometric parameters of the ion−ion docking differ by ~2% in the $O_{Ch}-O_{A1}$ distance and by 1% or less in the $N_{Ch}-O_{A2}$ distance.

Vibrational properties of the neutral pairs are similar to those of comparable organic/biological systems such as proteins or peptides.[47] To zero-order approximation, they can be characterized by stating that the vibrational density of states of each ion pair is the superposition of contributions from the separated cation and anion in their gas phase. Also in this case, a closer look at vibrational eigenvalues and eigenvectors shows a wealth of details that could guide the identification of species and configuration by spectroscopic means. At high frequency ($\geq$2800 cm^{-1}), the formation of the ion pair is accompanied by the drastic lowering of the stretching frequency of the OH termination of $[Chol]^+$. At low and medium frequencies, Coulomb interactions between cation and anion give rise to characteristic IR-active modes reminiscent of optical phonons in extended ionic systems. The oscillator strength expected for these vibrations, however, is fragmented into several different modes by the multiplicity of bare-Coulomb and polar interactions among different functional groups.

For all of the $[Chol]^+$ pairs that we considered, the energy of the lowest energy singlet electron excitation, computed by the ΔSCF method within the PBE+vdW approximation, falls in the UV range, with slight variations among the pairs that reflect the differences in the optical gap of the gas-phase anion. More precisely, computations of the excitation energy of cations and anions show that, as expected, the cation has the wider gap, roughly twice that of the anion. Given the fact that the two ionic moieties of each pair fully preserve their identity, it is not surprising to find that the low-energy excitations of the neutral pairs are simply a perturbed version of the anionic ones. Triplet excitation energies are ~0.7 eV lower than the corresponding singlet, again in line with the results of previous computations for a variety of organic systems.[56,57]

Replacing $[Chol]^+$ with its close analogue $[PhChol]^+$ has the effect of causing the transfer of the proton in the hydrogen bond from the cation to the anion, effectively neutralizing both species. This somewhat surprising result shows, first of all, that all of these systems are located in proximity of the Coulomb to polar transition, which, therefore, can be triggered by even modest perturbations. This fact alone makes these compounds interesting systems to study the interplay of ionicity and polarity in problems such as the solvation of organic molecules, the formation of electrified interfaces, and the ionic and proton conductivity in complex materials. It makes them also an ideal playground to study the protic character of ionic liquids.

The variety of behaviors that can be expected from these systems makes them interesting for a wide range of potential applications in electrochemistry, nanoionics, and polyelectrolyte solutions.[58] Compounds based on amino acids carrying additional acidic groups such as [Chol][Asp] could support a sizable proton conductivity in liquid and glassy phases, of potential interest for applications in photovoltaic devices, supercapacitors, batteries, and fuel cells.[59] In this respect, bistable hydrogen bonds and proton jumps are not the only requirement,[60] since genuine proton conductivity requires extended paths for the easy diffusion of protons across the system, as well as localized vibrational modes to assist protons in overcoming barriers. Large-scale ab initio computations for extended liquid and glassy phases are being planned to investigate these issues. The preliminary molecular dynamics simulations of small [Chol][Asp] clusters offer a first glimpse of the complex proton-transfer mechanisms that can be expected in larger systems.

Our study was meant to contribute to the ongoing discussion on room-temperature ionic liquids, providing the computational background to support the experimental characterization of a new wide class of such compounds.[18] Already at this stage, our results provide an intriguing view of these systems and point to several important features. For instance, the order of magnitude difference in the cohesive energy of the anion−cation pair and of larger aggregates made of neutral ion pairs easily accounts for the propensity of these systems to be liquid at ambient conditions.[18] On the other hand, this same observation suggests that, although ionic, these systems might display low dissociation and low ionic conductivity even in

dx.doi.org/10.1021/jp412281n | J. Phys. Chem. B 2014, 118, 2471−2486

condensed phases, consistently with the general picture of room-temperature ionic liquids proposed in ref 61. In the longer run, our data will be used to tune and validate classical force fields for large-scale molecular dynamics simulations of homogeneous liquid phases, whose results will be used together with X-ray diffraction data[18] for the iterative refinement of structural data on choline–amino acids RTILs, following the general approach detailed in in ref 62. Work along these lines is in progress.

The ab initio data will be of assistance also to improve the empirical modeling of a broader class of systems, since amino acids and choline or phosphocholine are reduced models for (parts of) more complex systems such as peptides, proteins, and lipids.[11−13] A short discussion of the relevance of our data to assess the validity of rigid-ion force-field models is deferred to the Supporting Information. It is worth mentioning, however, that several features of the systems that we investigated support the validity of such a description. Bond lengths and angles are well within the range found in charged or neutral organic compounds of similar composition, satisfactorily modeled by rigid-ion force fields.[63−65]

Other features apparently deviate from the rigid-ion force-field picture. First of all, atomic charges depend on the aggregation state of the ions under consideration, and, for instance, their absolute value increases when cation and anion are brought together to form a neutral ion pair. This effect saturates quickly with increasing cluster size, but it might still affect ions at the surface of even large aggregates. The corresponding re-distribution of charge within each ion represents a major component of the system polarization lying beyond the reach of rigid-ions models, and even of fixed-charge polarizable models,[66,67] even though it might be covered by recent fluctuating charge models.[68,69]

A further and major deviation from the rigid-ion force-field picture is represented by compounds such as [Chol][Asp] in which the proton transfer between different functional groups is an essential feature of the system dynamics. In principle, this effect could be modeled by reactive force fields,[70] but in this case the complexity of the model and of its parametrization represent a major difficulty, and the reliability of the approach still requires further validation.

As a last remark, we point out that the ab initio determination of low-lying electronic excitations for a number of homologous compounds might promote the development of simple models to predict or at least interpolate optical properties of finite and extended systems made of ionic organic compounds.

■ ASSOCIATED CONTENT

Supporting Information

Figures showing optimized geometry of the neutral ion pairs; tables listing ESP charges of cations, anions, and neutral pairs and vibrational eigenvectors and infrared activity of harmonic modes for all neutral ion pairs and text discussing the similarities and differences between ab initio and force-field modeling. This material is available free of charge via the Internet at http://pubs.acs.org.

■ AUTHOR INFORMATION

Corresponding Authors

*E-mail: enrico.bodo@uniroma1.it.

*E-mail: lorenzo.gontrani@gmail.com. Postal address: Department of Chemistry, Università di Roma "La Sapienza", P. Aldo Moro 5, 00185 Roma, Italy.

Notes

The authors declare no competing financial interest.

■ ACKNOWLEDGMENTS

A.B. acknowledges support from the European Community under the Marie Curie Intra-European Fellowship for Career Development (IEF) Grant No. 301463; E B. acknowledges the computational grants IscrB_METIL and IscrC_ESP-IL from Cineca; L.G. acknowledges support from FIRB RBFR086BOQ; P.B. acknowledges support from the Istituto Italiano di Tecnologia (IIT) under the SEED project SIMBEDD Grant No. 259; and R.C. acknowledges support from AWARDS_SAPIENZA (Grant C26H13MNEB).

■ REFERENCES

(1) Welton, T. Room-Temperature Ionic Liquids. Solvents for Synthesis and Catalysis. *Chem. Rev.* **1999**, *99*, 2071−2084.

(2) Brennecke, J. F.; Maginn, E. J. Ionic Liquids: Innovative Fluids for Chemical Processing. *AIChE J.* **2001**, *47*, 2384−2389.

(3) *Ionic Liquids: From Knowledge to Applications*; Plechkova, N. V., Rogers, R. D., Seddon, K. R., Eds.; ACS Symposium Series 1030; American Chemical Society: Washington, DC, USA, 2009.

(4) Holbrey, J.; Seddon, K. R. Ionic Liquids. *Clean Prod. Process.* **1999**, *1*, 223−236.

(5) Hough, W. L.; Smiglak, M.; Rodríguez, H.; Swatloski, R. P.; Spear, S. K.; Daly, D. Y.; Pernak, J.; Grisel, J. E.; Carliss, R. D.; Soutullo, M. D.; Davis, J. H., Jr.; Rogers, R. D. The Third Evolution of Ionic Liquids: Active Pharmaceutical Ingredients. *New J. Chem.* **2007**, *31*, 1429−1436.

(6) Stoimenovski, J.; Dean, P. M.; Izgorodina, E. I.; MacFarlane, D. R. Protic Pharmaceutical Ionic Liquids and Solids: Aspects of Protonics. *Faraday Discuss.* **2012**, *154*, 335−352.

(7) Fukumoto, K.; Yoshizawa, M.; Ohno, H. Room Temperature Ionic Liquids from 20 Natural Amino Acids. *J. Am. Chem. Soc.* **2005**, *127*, 2398−2399.

(8) Ohno, H.; Fukumoto, K. Amino Acid Ionic Liquids. *Acc. Chem. Res.* **2007**, *40*, 1122−1129.

(9) Dagade, D. H.; Madkar, K. R.; Shinde, S. P.; Barge, S. S. Thermodynamic Studies of Ionic Hydration and Interactions for Amino Acid Ionic Liquids in Aqueous Solutions at 298.15 K. *J. Phys. Chem. B* **2013**, *117*, 1031−1043.

(10) Kagimoto, J.; Taguchi, S.; Fukumoto, K.; Ohno, H. Hydrophobic and Low-Density Amino Acid Ionic Liquids. *J. Mol. Liq.* **2010**, *153*, 133−138.

(11) Weaver, K. D.; Van Vorst, M. P.; Vijayaraghavan, R.; MacFarlane, D. R.; Elliott, G. D. Interaction of Choline Salts with Artificial Biological Membranes: DSC Studies Elucidating Cellular Interactions. *Biochim. Biophys. Acta* **2013**, *1828*, 1856−1862.

(12) Weaver, K. D.; Kim, H.-J.; Sun, J.; MacFarlane, D. R.; Elliott, G. D. Cyto-toxicity and Biocompatibility of a Family of Choline Phosphate Ionic Liquids Designed for Pharmaceutical Applications. *Green Chem.* **2010**, *12*, 507−513.

(13) Rana, U. A.; Vijayaraghavan, R.; Doherty, C. M.; Chandra, A.; Efthimiadis, J.; Hill, A. J.; MacFarlane, D. R.; Forsyth, M. Role of Defects in the High Ionic Conductivity of Choline Triflate Plastic Crystal and Its Acid-Containing Compositions. *J. Phys. Chem. C* **2013**, *117*, 5532−5543.

(14) Abbott, A. P.; Boothby, D.; Capper, G.; Davies, D. L.; Rasheed, R. K. Deep Eutectic Solvents Formed between Choline Chloride and Carboxylic Acids: Versatile Alternatives to Ionic Liquids. *J. Am. Chem. Soc.* **2004**, *126*, 9142−9147.

(15) Tietze, A. A.; Bordusa, F.; Giernoth, R.; Imhof, D.; Lenzer, T.; MaaB, A.; Mrestani-Klaus, C.; Neundorf, I.; Oum, K.; Reith, D.; Stark, A. On the Nature of Interactions between Ionic Liquids and Small

Amino-Acid-Based Biomolecules. *ChemPhysChem* **2013**, *14*, 4044−4064.
(16) Chen, X.; Liu, J.; Wang, J. Ionic Liquids in the Assay of Proteins. *Anal. Methods* **2010**, *2*, 1222−1226.
(17) *ILs in Biotransformations and Organocatalysis: Solvents and Beyond*; Dominguez de Maria, P., Ed.; Wiley: Hoboken, NJ, USA, 2012.
(18) Ionic compounds consisting of a choline cation and an amino acid anion have been synthesysed by: Caminiti, R.; Sferrazza, A., Dipartimento di Chimica, Universita di Roma "La Sapienza". These compounds appear to be liquid at ambient conditions (private communication).
(19) Angell, C. A.; Byrne, N.; Belieres, J.-P. Parallel Developments in Aprotic and Protic Ionic Liquids: Physical Chemistry and Applications. *Acc. Chem. Res.* **2007**, *40*, 1228−1236.
(20) Dommert, F.; Wendler, K.; Qiao, B.; Delle Site, L.; Holm, C. Generic Force Fields for Ionic Liquids. *J. Mol. Liq.* **2014**, in press.
(21) Canongia Lopes, J. N.; Padua, A. A. H. A Generic and Systematic Force Field for Ionic Liquids Modeling. *Theor. Chem. Acc.* **2012**, *131*, 1129−1139.
(22) Köddermann, T.; Reith, D.; Ludwig, R. Comparison of Force Fields on the Basis of Various Model Approaches—How To Design the Best Model for the [CnMIM][NTf2] Family of Ionic Liquids. *ChemPhysChem* **2013**, *14*, 3368−3374.
(23) Martin, R. M. *Electronic Structure, Basic Theory and Practical Methods*; Cambridge University Press: Cambridge, U.K., 2004.
(24) CPMD version 3.15.3, Copyright IBM Corp, 1990−2008; Copyright MPI für Festkörperforschung Stuttgart, 1997−2001. http://www.cpmd.org/.
(25) Troullier, N.; Martins, J. L. Efficient Pseudopotentials for Plane Wave Computations. *Phys. Rev. B* **1991**, *43*, 1993−2006.
(26) Martyna, G. J.; Tuckerman, M. E. A Reciprocal Space Based Method for Treating Long Range Interactions in ab-Initio and Force-Field-Based Calculations in Clusters. *J. Chem. Phys.* **1999**, *110*, 2810−2821.
(27) Perdew, J. P.; Burke, K.; Ernzerhof, M. Generalized Gradient Approximation Made Simple. *Phys. Rev. Lett.* **1996**, *77*, 3865−3568.
(28) Grimme, S. Semiempirical GGA-Type Density Functional Constructed with a Long-Range Dispersion Correction. *J. Comput. Chem.* **2006**, *27*, 1787−1799.
(29) Frisch, M. J.; Trucks, G. W.; Schlegel, H. B.; Scuseria, G. E.; Robb, M. A.; Cheeseman, J. R.; Scalmani, G.; Barone, V.; Mennucci, B.; Petersson, G. A.; et al. *Gaussian 09*, Revision D.01; Gaussian: Wallingford, CT, USA, 2009.
(30) Zhao, Y.; Truhlar, D. G. The M06 Suite of Density Functionals for Main Group Thermochemistry, Thermochemical Kinetics, Non-Covalent Interactions, Excited States, and Transition Elements. *Theor. Chem. Acc.* **2008**, *120*, 215−241.
(31) Grimme, S.; Antony, J.; Ehrlich, S.; Krieg, H. A Consistent and Accurate ab-Initio Parametrization of Density Functional Dispersion Correction (DFT-D) for the 94 Elements H-Pu. *J. Chem. Phys.* **2010**, *132*, 154104.
(32) The choice of the M06-2X/D3 combination has been guided by the results of: Zahn, S.; MacFarlane, D. R.; Izgorodina, E. I. Assessment of Kohn−Sham Density Functional Theory and MollerPlesset Perturbation Theory for Ionic Liquids. *Phys. Chem. Chem. Phys.* **2013**, *15*, 13664−13675.
(33) Li, X.; Frisch, M. J. Energy-Represented Direct Inversion in the Iterative Subspace within a Hybrid Geometry Optimization Method. *J. Chem. Theory Comput.* **2006**, *2*, 835−839.
(34) Singh, U. C.; Kollman, P. A. An Approach to Computing Electrostatic Charges for Molecules. *J. Comput. Chem.* **1984**, *5*, 129−145.
(35) Reed, A. E.; Curtis, L. A.; Weinhold, F. A. Intermolecular Interactions from a Natural Bond Orbital, Donor−Acceptor Viewpoint. *Chem. Rev.* **1988**, *88*, 899−926.
(36) Weinhold, F. Nature of H-Bonding in Clusters, Liquids, and Enzymes: An ab-Initio, Natural Bond Orbital Perspective. *J. Mol. Struct. (THEOCHEM)* **1997**, *398*−*399*, 181−197.
(37) Löwdin, P. O. Quantum Theory of Many-Particle Systems. I. Physical Interpretations by Means of Density Matrices, Natural Spin-Orbitals, and Convergence Problems in the Method of Configurational Interaction. *Phys. Rev.* **1955**, *97*, 1474−1489.
(38) We use the SHAKE algorithm implemented in CPMD to carry out the constrained energy minimisation; see: Ryckaert, J.-P.; Ciccotti, G.; Berendsen, H. J. C. Numerical Integration of Cartesian Equations of Motion of a System with Constraints. *J. Comput. Phys.* **1997**, *23*, 327−341.
(39) Ziegler, T.; Rauk, A.; Baerends, E. J. Calculation of Multiplet Energies by Hartree-Fock-Slater Method. *Theor. Chim. Acta* **1977**, *43*, 261−271.
(40) von Barth, U. Local-Density Theory of Multiplet Structure. *Phys. Rev. A* **1979**, *20*, 1693−1703.
(41) Frank, I.; Hutter, J.; Marx, D.; Parrinello, M. Molecular Dynamics in Low-Spin Excited States. *J. Chem. Phys.* **1998**, *108*, 4060−4069.
(42) Kowalczyk, T.; Yost, S. R.; Van Voorhis, T. Assessment of the Delta SCF Density Functional Theory Approach for Electronic Excitations in Organic Dyes. *J. Chem. Phys.* **2011**, *134*, 054128.
(43) Casida, M. E. Time-Dependent Density-Functional Response Theory for Molecules. In *Recent Advances in Density-Functional Methods*; Chong, D. P., Ed.; World Scientific: Singapore, 1995; pp 155−192.
(44) Onida, G.; Reining, L.; Rubio, A. Electronic Excitations: Density-Functional Versus Many-Body Greens-Function Approaches. *Rev. Mod. Phys.* **2002**, *74*, 601−659.
(45) Huggins, M. L. Hydrogen Bridges in Ice and Liquid Water. *J. Phys. Chem.* **1936**, *40*, 723−731. Kreuer, K.-D. Proton Conductivity: Materials and Applications. *Chem. Mater.* **1996**, *8*, 610−641.
(46) Marx, D.; Tuckerman, M. E.; Hutter, J.; Parrinello, M. The Nature of the Hydrated Excess Proton in Water. *Nature* **1999**, *397*, 601−604.
(47) *Infrared Analysis of Peptides and Proteins*; Singh, B. R., Ed.; ACS Symposium Series 750; American Chemical Society: Washington, DC, USA, 2000.
(48) Paul, A.; Mandal, P. K.; Samanta, A. On the Optical Properties of the Imidazolium Ionic Liquids. *J. Phys. Chem. B* **2005**, *109*, 9148−9153.
(49) Hunt, P. A.; Kirchner, B.; Welton, T. Characterising the Electronic Structure of Ionic Liquids: An Examination of the 1-Butyl-3-Methylimidazolium Chloride Ion Pair. *Chem.—Eur. J.* **2006**, *12*, 6762−6775.
(50) Goldfarb, A. R.; Saidel, L. J.; Mosovich, E. The Ultraviolet Absorption Spectra of Proteins. *J. Biol. Chem.* **1951**, *193*, 397−404.
(51) The triplet excitations are forbidden in our nonrelativistic computations.
(52) Berendsen, H. J. C.; Postma, J. P. M.; van Gunsteren, W. F.; DiNola, A.; Haak, J. R. Molecular Dynamics with Coupling to an External Bath. *J. Chem. Phys.* **1984**, *81*, 3684−3690.
(53) We display the probability distribution instead of a radial distribution function because the system is far from being homogeneous and isotropic.
(54) Weis, J. J.; Levesque, D. Chain Formation in Low-Density Dipolar Hard-Spheres: A Monte Carlo Study. *Phys. Rev. Lett.* **1993**, *71*, 2729−2732.
(55) Law, G.; Watson, P. R. Surface Tension Measurements of *N*-Alkylimidazolium Ionic Liquids. *Langmuir* **2001**, *17*, 6138−6141.
(56) Zhao, X.; Chen, M. A TDDFT Study on the Singlet and Triplet Excited-State Hydrogen Bonding and Proton Transfer of 10-Hydroxybenzo[h]Quinoline (HBQ) and 7,9-Diiodo-10-Hydroxybenzo[h]Quinoline (DIHBQ). *Chem. Phys. Lett.* **2011**, *512*, 35−39.
(57) Fabiano, E.; Della Sala, F.; Cingolani, R.; Weimer, M.; Görling, A. Theoretical Study of Singlet and Triplet Excitation Energies in Oligothiophenes. *J. Phys. Chem. A* **2005**, *109*, 3078−3085.
(58) Rana, U. A.; Forsyth, M.; MacFarlane, D. R.; Pringle, J. M. Toward Protic Ionic Liquid and Organic Ionic Plastic Crystal Electrolytes for Fuel Cells. *Electrochem. Acta* **2012**, *84*, 213−222.

(59) Winter, M.; Brodd, R. J. What are Batteries, Fuel Cells, and Supercapacitors? *Chem. Rev.* **2004**, *104*, 4245−4269.
(60) Kreuer, K.-D.; Paddison, S. J.; Spohr, E.; Schuster, M. Transport in Proton Conductors for Fuel-Cell Applications: Simulations, Elementary Reactions, and Phenomenology. *Chem. Rev.* **2004**, *104*, 4637−4678.
(61) Gebbie, M. A.; Valtiner, M.; Banquy, X.; Fox, E. T.; Henderson, W. A.; Israelachvili, J. N. Ionic Liquids Behave as Dilute Electrolyte Solutions. *Proc. Natl. Acad. Sci. U. S. A.* **2013**, *110*, 9674−9679.
(62) Kashyap, H. K.; Santos, C. S.; Annapureddy, H. V. R.; Murthy, N. S.; Margulis, C. J.; Castner, E. W., Jr. Temperature-Dependent Structure of Ionic Liquids: X-Ray Scattering and Simulations. *Faraday Discuss.* **2012**, *154*, 133−143.
(63) Canongia Lopes, J. N.; Deschamps, J.; Padua, A. A. H. Modeling Ionic Liquids Using a Systematic All-Atom Force Field. *J. Phys. Chem. B* **2004**, *108*, 2038−2047. Additions and Corrections: Canongia Lopes, J. N.; Deschamps, J.; Padua, A. A. H. *J. Phys. Chem. B* **2004**, *108*, 11250.
(64) Cornell, W. D.; Cieplak, P.; Bayly, C. I.; Gould, I. R.; Merz, K. M.; Ferguson, D. M.; Spellmeyer, D. C.; Fox, T.; Caldwell, J. W.; Kollman, P. A. A Second Generation Force Field for the Simulation of Proteins, Nucleic Acids, and Organic Molecules. *J. Am. Chem. Soc.* **1995**, *117*, 5179−5197.
(65) Brooks, B. R.; Brooks, C. L., 3rd; Mackerell, A. D., Jr.; Nilsson, L.; Petrella, R. J.; Roux, B.; Won, Y.; Archontis, G.; Bartels, C.; Boresch, S. CHARMM: The Biomolecular Simulation Program. *J. Comput. Chem.* **2009**, *30*, 1545−1614.
(66) Yan, T. Y.; Burnham, C. J.; Del Popolo, M. G.; Voth, G. A. Molecular Dynamics Simulation of Ionic Liquids: The Effect of Electronic Polarizability. *J. Phys. Chem. B* **2004**, *108*, 11877−11881.
(67) Salanne, M.; Rotenberg, B.; Jahn, S.; Vuilleumier, R.; Simon, C.; Madden, P. A. Including Many-Body Effects in Models for Ionic Liquids. *Theor. Chem. Acc.* **2012**, *131*, 1143−1149.
(68) Patel, S.; Brooks, C. L., III. CHARMM Fluctuating Charge Force Field for Proteins: I Parameterization and Application to Bulk Organic Liquid Simulations. *J. Comput. Chem.* **2004**, *25*, 1−15.
(69) Bingham, R.; Ballone, P. Energy, Structure and Vibrational Modes of Small Water Clusters by a Simple Many-Body Potential Mimicking Polarisation Effects. *Mol. Phys.* **2013**, *111*, 3502−3514.
(70) van Duin, A. C. T.; Dasgupta, S.; Lorant, F.; Goddard, W. A. ReaxFF: A Reactive Force Field for Hydrocarbons. *J. Phys. Chem. A* **2001**, *105*, 9396−9409.